Journal of Materials Chemistry A

Accepted Manuscript

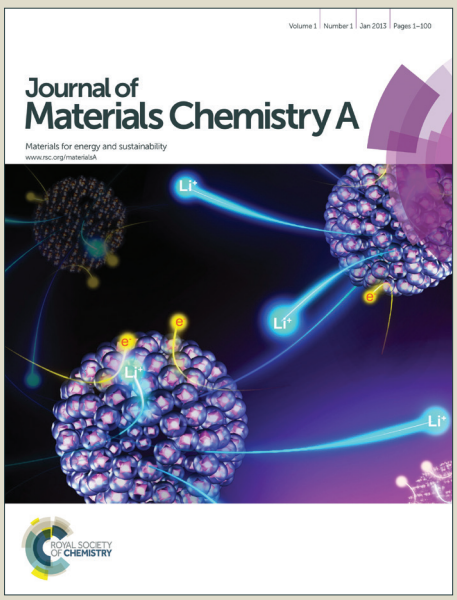

ROYAL SOCIETY OF CHEMISTRY

www.rsc.org/materialsA

Three-dimensional α-Fe_2O_3/carbon nanotube sponges as flexible supercapacitor electrodes

Xiaoping Cheng[1], Xuchun Gui[1,*], Zhiqiang Lin[1], Yongjia Zheng[1], Ming Liu[1], Runze Zhan[1], Yuan Zhu[1] and Zikang Tang[1, 2]

[1] *State Key Lab of Optoelectronic Materials and Technologies, School of Physics and Engineering, Sun Yat-sen University, Guangzhou, 510275, P. R. China*

[2]*Institute of Applied Physics and Materials Engineering, University of Macau, Avenida da Universidade, Taipa, Macau, China*

Corresponding authors: guixch@mail.sysu.edu.cn;

Abstract

Flexible supercapacitors, which can sustain large deformations while maintaining normal functions and reliability, are playing an increasingly important role in portable electronics. Here we report the preparation of a three-dimensional α-Fe_2O_3/carbon nanotube (CNT@Fe_2O_3) sponge electrode with a porous hierarchical structure, consisting of a compressible, conductive CNT network, coated with a layer of Fe_2O_3 nanohorns. The specific capacitance of these hybrid sponges has been significantly improved to above 300 F/g, while the equivalent series resistance remains at about 1.5 Ω. The highly deformed CNT@Fe_2O_3 sponge retains more than 90 % of the original specific capacitance under a compressive strain of 70% (corresponding to a volume reduction of 70%). The hybrid sponge still works stably and sustains similar specific capacitance as initial value even after 1000 compression cycles at a strain of 50%. The outstanding properties of this hybrid sponge make it a highly promising candidate for flexible energy devices.

1. Introduction

Recent advances in foldable, compressible, and stretchable electronics have promoted increasing demand for lightweight, and flexible high-performance power sources that can sustain large deformations while maintaining normal functions and reliability.[1-4] As for energy storage devices, electrochemical supercapacitors store energy through double-layers capacitance and pseudocapacitance, providing a high power density and modest energy density system.[1, 5] Experimental results suggest that the electrode material plays a key role in the development of high performance supercapacitors.[6-7] Among various supercapacitor electrode materials, carbon based nanomaterials (such as carbon nanotubes (CNTs), and graphene), which typically store energy through an electric double-layer effect at the electrode/electrolyte interface, have received extensive attention owing to their high specific surface area, excellent electrical conductivity, and environmental friendliness.[8-11] However, the relatively low specific capacitance (or energy density) is far from satisfaction. Therefore, it is highly desirable to explore new electrode materials.

Pseudocapacitive materials (including transition-metal oxides and electrically conducting polymers) with higher energy density have been hybridized with carbon materials to improve the performance of electrode materials. For example, the specific capacitance of CNT increased about 2-11 times when grafted with RuO_2 (6.7 times), MnO_2 (7.7 times), V_2O_5 (6.4 times), Co_4O_3 (2.2 times), or PPy(10.7 times).[12-16] Among these oxides, iron oxides are considered as particularly promising electrode materials because of their variable oxidation states, natural abundance, low cost, low toxicity, and high theoretical capacity.[17-23] Different electrode composites have been constructed form carbon based materials and iron

oxides, such as nanocomposite of goethite nanorods and reduced graphene oxide, graphite-like C_3N_4 hybridized α-Fe_2O_3 hollow microspheres, 2D sandwich-like graphene-supported Fe_3O_4, and graphene/Fe_2O_3 hydrogels.[24-27] Typically, these materials are in powder form and have a specific capacitance of 100~250 F/g. [17-23] When used in supercapacitors, these active materials are mixed with conductive additives and binders on a metal current collector to form the electrode. However, electrodes assembled using these methods rarely display good mechanical properties, which are necessary for flexible electrodes. Recently reports on new types of freestanding carbon-based 3D architectures such as aerogels, foams, and sponges have revealed further improved mechanical properties of the electrodes.[1,3,28-30] However, there has been limited progress in developing flexible supercapacitors.

Here we report an effective approach to fabricate a porous electrode, in which carbon nanotube sponge was uniformly coated with α-Fe_2O_3 nanohorns (CNT@Fe_2O_3), and demonstrate the application of the hybrid sponge as a highly compressible supercapacitor electrode. The pseudocapacitive material (α-Fe_2O_3) was directly deposited into the 3D porous sponge by low-temperature hydrothermal synthesis, while protecting the original interconnected CNT network and high conductivity. Furthermore, the monolithic material can directly act as the current collector, leading to a lighter weight and higher energy density than the 3D carbon powder nanostructures. Furthermore, the CNT@Fe_2O_3 sponges maintain stable electrochemical characteristics under high compression, which confirms their potential use as flexible electrodes.

2. Experimental

2.1 Fabrication of CNT @α-Fe_2O_3 sponges

CNT sponges were synthesized by CVD, as reported by our group previously.[31] To fabricate the α-Fe_2O_3/CNT composite, the as-grown CNT sponges were cut into rectangular blocks (about 8 ×6 ×3 mm^3) and exposed to UV for 1 hour. The obtained sponge blocks were immersed into 30 mL $FeCl_3$ ethanol/aqueous precursor solution with a concentration in the range 0.01-1.0 M (the volume rate of ethanol and aqueous was 1:1). The mixture was sealed in a 50 mL Telfon-lined autoclave and hydrothermally treated at 100℃ for 2 h. Then, the CNT@FeOOH sponges were taken out, washed repeatedly with deionized water, and freeze-dried. At last, the composite was annealed in air by an atmospheric pressure tubular furnace to obtain α-Fe_2O_3/CNT sponges. The annealed temperature and time were 300℃ and 3 hours. The heating rate was set as 10 ℃ min^{-1}.

2.2 Characterization

Scanning electron microscopy (SEM, S-4800), transmission electron microscopy (TEM, JEM-2010HR), and an X-ray diffraction (XRD) (Empyrean) were used to characterize the morphology and structure of sample. Raman spectra were performed on a high resolution confocal Raman spectrometer (LabRAM HR) with a 633 nm laser. X-ray photoelectron spectroscopy (XPS) was recorded using an ESCALAB 250Xi spectrometer. Thermogravimetric analysis (TGA) was conducted on a simultaneous thermal analyzer coupled with Fourier transform infrared spectrometry (STA449F3) from 20 to 800℃ in air atmosphere at a heating rate of 20℃/min. Mechanical tests were carried out by an electronic

universal testing machine (Instron 5943) equipped with two flat-surface compression stages.

2.3 Electrochemical measurement

All the electrochemical experiments were carried out in 2 M KCl aqueous electrolyte at room temperature using Zahner electrochemical station. Cyclic voltammetry (CV), galvanostatic charge/discharge, and electrochemical impedance spectroscopy (EIS) were measured in a standard three-electrode system with platinum wire and saturated Ag/AgCl electrode as the counter and reference electrode. The sponge clamped by two polymeric blocks (twisted around by platinum wire) was used as working electrode. The CV curves were measured under different scan rates of 5-300 mV/s between -1 and 0 V. EIS measurements were carried out in the frequency range from 100 kHz to 0.1 Hz at open circuit potential with an ac perturbation of 5 mV. The specific capacitance of the supercapacitor was calculated from the CV curves according to the following equation:

$$C_s = \frac{\int IdV}{m\nu\Delta V}$$

where I is the response current (A), V is the potential vs Ag/AgCl, m is the mass of electrode (g), ν is the potential scan rate (mV/s), ΔV is the potential range (V).

3. Results and Discussion

Our strategy is to deposit uniform and porous Fe_2O_3 nanoparticles within the CNT sponge, while maintaining its original 3D network and mechanical stability, as illustrated in Fig. 1(a). First, the CNT sponge was immersed in precursor $FeCl_3$ solution to deposit FeOOH

nanospindles on the surface of the CNT by a low temperature hydrothermal process, resulting in a hierarchical CNT@FeOOH sponge. Prior to this growth, the CNT sponges were treated with UV/O_3 to increase their hydrophilicity. The CNTs contain many oxygen-containing groups and other carbon hexagonal ring after the UV treatment.[32, 33] These groups on CNTs can act as anchoring sites or nucleation sites for the growth of FeOOH.[34] As a result, the FeOOH nanoparticles spontaneously grow and uniformly assemble on the entire surface of each nanotube. Subsequently, the CNT@FeOOH sponge was annealed in air to convert it to CNT@Fe_2O_3 sponge, as verified by the thermogravimetric analysis of CNT@FeOOH (Fig. S1). The resulting CNT@Fe_2O_3 sponge maintained the porosity and flexibility of the original CNT sponges. It can be compressed to large strains and recovered to its initial shape. These characteristics are favorable for flexible supercapacitor application.

We have characterized the morphology of CNT and CNT@Fe_2O_3 sponges by SEM and TEM. The as-grown CNT sponge (inset of Fig. 1b) exhibits a well-defined interconnected 3D porous network (Fig. 1b). This porous structure is favorable for depositing pseudocapacitive materials by hydrothermal processes or in-situ polymerization, as the precursor solution could easily infiltrate into the inner portion of the sponge through the pores. [13, 16, 35] After deposition of FeOOH, the CNTs among the entire inner of sponge were uniformly decorated with nanospindles with a length of around 20-30 nm and diameter of 10 nm (Fig. 1c). The morphology of FeOOH is very sensitive to growth environment. It tends to form spindle-like shape in acid solution; however, rod-like FeOOH is the dominant shape in neutral solution.[36] Here, spindle-like FeOOH is more easily formed in ethanol/aqueous precursor solution (with a pH of 1.32-1.62). By careful annealing in air, the FeOOH nanospindles were converted to

Fe_2O_3 nanohorns (Fig. 1d). Because the CNTs form a stable skeleton, the CNT composite maintained its overall structure during the phase transformation of FeOOH (inset of Fig. 1d). TEM images reveal that the Fe_2O_3 nanoparticles become porous but the size and shape exhibit nearly no changes after annealing (Fig. 1e and 1f). Thermal dehydroxylation of FeOOH takes place during the annealing process while the morphology keeps the same in the conversion. The formation of the hollow structure is due to the volume reduction from the transformation of β-FeOOH with a low density of 3 g/cm^3 to denser α-Fe_2O_3 with a density of 5.3 g/cm^3.[37] Fe_2O_3 nanoparticles and CNT also show strong adhesive force. Fe_2O_3 nanoparticles were still adhered to CNTs, even after ultrasonic for 10 minutes.

More structural and phase characterizations of the CNT@Fe_2O_3 were investigated by X-ray diffraction (XRD) (Fig. 2a). The XRD pattern of the CNT@FeOOH corresponds well to that of β-FeOOH (JCPDS 42-1315) (Fig. 2a). After annealing, all diffraction peaks of the XRD pattern can be indexed to rhombohedral hematite structure (α-Fe_2O_3, JCPDF 33-0664), signifying the successful conversion of β-FeOOH to α-Fe_2O_3 during annealing. With a closer examination of its chemical composition, we carried out Raman and the X-ray photoelectron spectroscopy (XPS) analysis. The Raman spectrum of the CNT@Fe_2O_3 nanocomposite shows several characteristic peaks at 214, 273, 388, 478 and 584 cm^{-1} from α- Fe_2O_3, whereas the D and G peaks resulting from CNT were also observed (Fig. 2b). Furthermore, the XPS survey spectrum (Fig. 2c) demonstrates the coexistence of Fe, O, and C in the nanocomposite. In high-resolution XPS spectra of Fe2p region (insert in Fig. 2d), two obvious peaks at 710.2 and 723.9 eV are observed and corrspond to the $Fe2p_{3/2}$ and $Fe2p_{1/2}$ spin-orbit of Fe_2O_3. In addition to these two peaks, a satellite peak is observed at 719.3 eV, which is consistent with

the characterization of Fe^{3+}.[27, 38] TGA measurement carried out in air was used to determine the loading amount of Fe_2O_3 in the CNT@Fe_2O_3 sponge. As shown in Fig. 2d, the TGA curves display a significant loss of mass at approximately 550 ℃ and a constant weight above 650 ℃. The major weight loss from 550 to 650 ℃ resulted from the combustion of CNT. For the CNT sponge, the mass percent of the residue is about 18.0 %. This residue is attributed to the catalyst in the CNT during synthesis.[32] The content of Fe_2O_3 in CNT@Fe_2O_3 sponge was calculated to be 28.8, 47.0 and 72.0 wt. % for the samples grown at 0.01, 0.1 and 1.0 mol/L $FeCl_3$ solution, respectively.

During the assembly of FeOOH on the CNT sponge, the electrostatic adsorption of Fe^{3+} ions to oxygen-containing groups on CNTs and further hydrolysis, olation/oxolation may be responsible for the heterogeneous nucleation, growth of FeOOH nanospindles, and adhesion on the CNT network, as reported by Lou.[34] The Fe_2O_3 nanoparticles loading (18.0-72.0 wt. %) relative to the CNT mass and the morphology of Fe_2O_3 can be readily tuned by varying the initial concentration of $FeCl_3$ in solution and the hydrolysis period. The loading amount of Fe_2O_3 in the composite increased with the increasing concentration of the precursor, as can be seen from the TGA curves and SEM images (Fig. 2d and Fig. S2). However, when the concentration of $FeCl_3$ solution exceeded 0.1 mol/L or the hydrolysis period exceeded 4 hours, the Fe_2O_3 nanoparticles could agglomerate (Fig. S2 and Fig. S3).

To evaluate the supercapacitor performance of as-prepared CNT@Fe_2O_3 sponges, CV, galvanostatic charge/discharge, and EIS measurements were performed in a three-electrode configuration. Fig. 3a shows the CV curves collected at different scan rates from 5 to 300 mV/s in the voltage window of -1 to 0 V vs. Ag/AgCl (for use as negative electrodes in

aqueous electrochemical capacitors). The nearly mirror-image current response upon voltage reversal indicates good reversibility behavior of our nanocomposite electrode. The slight distortion of the rectangular shape manifests pseudocapacitive behavior of Fe_2O_3, which might arise from a reversible Fe^{3+}/Fe^{2+} couple.[39, 40] The specific capacitance calculated from the CV curves (Fig. 3a) is 296.3 F/g at a scan rate of 5 mV/s, which is much larger than those of the CNT sponge and Fe_2O_3. Cycling stability of the CNT@Fe_2O_3 electrode was investigated at a scan rate of 100 mV/s for 1000 cycles (Fig. 3b). There was a certain degree of degradation in the current density and specific capacitance after the first 200 charge and discharge cycles (maintaining about 80% of the initial value), similar to Fe_2O_3 composites reported previously.[17, 19, 21] After 1000 charge and discharge cycles, it still maintained more than 60% of the initial specific capacitance. Galvanostatic charge/discharge analyses were performed in the potential range of -1 to 0 V at different current densities between 1 and 20 A/g (Fig. S4). It shows symmetrical triangle curves revealing good reversibility of the CNT@Fe_2O_3 sponge electrode. Additionally, negligible voltage drop (IR drop) can be seen from the curves, indicating a very low internal resistance, which is important for energy strorage electrodes.

Fig. 3c compares the CV of the original CNT sponge and CNT@Fe_2O_3 sponges at the same scan rate of 100 mV/s. The CNT@Fe_2O_3 sponges are prepared at different concentrations of $FeCl_3$ solution (0.01, 0.1 and 1.0 mol/L). The CV curves of the original CNT sponge exhibits a typical nearly rectangular shape, suggesting fast reversible Faradic reactions and electrical double-layer capacitor behavior.[28] Two small redox peaks were also observed at -0.5V. Considering the oxygen-containing groups originating from the UV/O_3

irradiation, we suppose that an oxidation or reduction reaction has taken place during the CV scan. In comparison, the Fe_2O_3 decoration leads to higher current density and enlarged area enclosed by the CV curve, which obviously demonstrates the pseudocapacitance of Fe_2O_3 nanospindles. Fig. 3d is a summary plot of specific capacitance at different CV scan rates. The highest specific capacitance is about 296.3 F/g obtained for the CNT@Fe_2O_3 sponge (grown at a concentration of 0.1 mol/L) at a scan rate of 5 mV/s, compared with the CNT sponge (80.2 F/g) and the CNT@Fe_2O_3 grown at 0.01 mol/L (177.3 F/g) and 1.0 mol/L (264.6 F/g). The higher specific capacitance of the CNT@Fe_2O_3 sponges results from the combination of the electric double-layer capacitance of the porous CNT network and the pseudocapacitance of Fe_2O_3. When more active material (Fe_2O_3) is anchored to the CNT surface, the faradic current of the supercapacitor electrode becomes stronger. At low growth concentration (lower than 0.1 mol/L), the capacitance of the samples increased almost linearly (inset of Fig. 3d). However, increasing of the Fe_2O_3 loading does not lead to a continued improvement in specific capacitance due to the increase in the overall weight and a decrease in homogeneous distribution of the nanoparticles. We can clearly observe a larger crystal size of the Fe_2O_3 (80-100 nm for 1.0 mol/L sample), and aggregation of the nanohorns. This may directly leads to a decrease of specific surface area, as well as the electronic and the ionic charge separation rate at the electrode-electrolyte interfaces, which can explain the inferior specific capacitance of the 1.0 mol/L sample compared with the 0.1 mol/L sample. From galvanostatic charge/discharge measurements (Fig. 3e), the CNT@Fe_2O_3 sponges have a longer charging and discharging time than the pristine sponge, illustrating their larger capacitance, which corroborates the result from the CV curve. Fig. 3f shows the Nyquist plots

of the EIS spectra for different samples. All spectra show a semicircle in the high frequency range and a straight sloping line in the low frequency range. The equivalent series resistance (R_s), read at the intercept of the semicircle on the Z' axis at high frequency, are approximately equal for all samples (~1.5 Ω). Additionally, the diameter of the semicircle represents the charge-transfer resistance (R_{ct}) for the electrode. The R_{ct} of CNT@Fe_2O_3 sponges is about 2.0 Ω, a little higher than that of original CNT sponge (1.1 Ω) and much lower than that of Fe_2O_3 (10 Ω),[41] demonstrating good combination of the CNT and Fe_2O_3. The four straight lines at the low frequency range exhibiting a similar slope (nearly vertical) suggest good capacitive behavior without diffusion limitation.

Besides the improvement of specific capacitance by doping with Fe_2O_3, the CNT@Fe_2O_3 sponges still maintain their flexibility and recover under large degree compression (inset of Fig. 4d). Five CNT@Fe_2O_3 sponges (fabricated at the same conditions) were measured in the original state and compressive state with a strain of 10%, 30%, 50% and 70%, respectively. At the same scan rate of 5 mV/s, the sponges showed similar CV curves and specific capacitance under the different compressions (Fig. 4a). The highly deformed sponge electrode retained above 90% of the original specific capacitance even up to 70% reduction of its volume. A similar conclusion is conveyed without distinct change at different strain *via* the galvanostatic charge/discharge results (Fig. 4b). The equivalent series resistance (R_s) of the electrode stayed the same regardless of the increasing strain, while the charge-transfer resistance (R_{ct}) gets moderately bigger from 1.9 to 2.8 Ω as the strain increases from 0 to 70% (Fig. 4c). For the CNT@Fe_2O_3 sponge, the CNT network acts as a reinforced skeleton and provides the main mechanical strength. Even with intensive volume

reduction, the 3D CNTs can maintain an open porous structure to allow electrolyte infiltration, which is important for ion diffusion and minimizing capacity loss.[28] After 1000 cycles of compression under 50% strain, the CNT@Fe_2O_3 sponge shows similar CV curves (Fig. 4d) and Nyquist plot (Fig. S5) compared with the original state at a scan rate of 5 mV/s. At high scan rate (100 mV/s), it also shows the same characters (Fig. S6). Stress-strain curves reveal that the CNT@Fe_2O_3 sponge can recover most of its volume during the unloading stage with negligible plastic deformation (Fig. S7). This indicates that the hybrid sponge can work as a stable compressible electrode and sustain repeated deformation for many compression cycles.

To further understand the materials stability, which is directly related to electrochemical cyclic stability, morphology and structure analysis was conducted on the sample after a 1000 cycles test at a scan rate of 1000 mV/s. From the typical SEM images showed in Fig. 5a and 5b, one can see that the rice-like Fe_2O_3 nanohorns have changed into spherical particles, and that the primary particles are slightly aggregated and have grown to 30 nm in size; this is because of the formation of a solid electrolyte interphase layer.[42, 43] Similar aggregation of Fe_2O_3 nanoparticles in electrochemical reactions has also been observed by Lu etc.[19] Meanwhile, the similar Raman spectrum (Fig. 5c) and similar binding energy (Fig. 5d) and XRD (Fig. S8) indicate that the crystalline structure of α-Fe_2O_3 did not change. The spheroidizing and aggregation of the Fe_2O_3 could lead to a decrease of the specific surface area of the active materials and an increase of the ion diffusion distance, resulting in the attenuation of capacitor during electrochemical cycle.

4. Conclusion

A freestanding three-dimensional composite based on a CNT sponge and grafted Fe_2O_3 crystals is constructed. As a pseudocapacitive material, Fe_2O_3 involves a relatively rapid and reversible redox reaction during the charge/discharge process, which remarkably improves the capacitance of sponge electrode. The electric double-layer capacitance and pseudocapacitance jointly account for the high specific capacitance of the as-prepared CNT@Fe_2O_3 sponge. Furthermore, the significant compressibility and robustness arising from the CNTs sponge skeleton protect the hybrid material from performance degradation under large strain for many cycles. It is believed that the rationally designed composite material can afford a better overall performance in light-weight and flexible energy devices.

Acknowledgments

This work was partially supported by Guangdong Natural Science Funds for Distinguished Young Scholar (Grant No: 2014A030306022), Pearl River Rising Star Program (No. 2014J2200066).

Electronic supplementary information (ESI) available: TGA of CNT@FeOOH sponge. SEM images of the CNT@Fe_2O_3 sponges grown at different $FeCl_3$ precursor concentration, and hydrothermal time. Galvanostatic charge/discharge curves of CNT@Fe_2O_3 sponge. CV curves and Nyquist plot of CNT@Fe_2O_3 sponge before and after 1000 compression cycles. Compressive stress-strain curves of CNT@Fe_2O_3 sponge.

Notes and References

1. K. Xie and B. Wei, Materials and Structures for Stretchable Energy Storage and Conversion Devices, *Adv. Mater.*, 2014, **26**, 3592-3617.

2. G. Zhou, F. Li and H. M. Cheng, Progress in Flexible Lithium Batteries and Future Prospects, *Energy Environ. Sci.*, 2014, **7**, 1307-1338.
3. T. Chen, H. Peng, M. Durstock and L. Dai, High-Performance Transparent and Stretchable All-Solid Supercapacitors Based on Highly Aligned Carbon Nanotube Sheets, *Sci. Rep.*, 2014, **4**, 3612.
4. Y. Yang, G. Ruan, C. Xiang, G. Wang and J. M. Tour, Flexible Three-Dimensional Nanoporous Metal-Based Energy Devices, *J. Am. Chem. Soc.*, 2014, **136**, 6187-6190.
5. J. R. Miller and P. Simon, Electrochemical Capacitors for Energy Management, *Science*, 2008, **321**, 651-652.
6. G. Wang, L. Zhang and J. Zhang, A Review of Electrode Materials for Electrochemical Supercapacitors, *Chem. Soc. Rev.*, 2012, **41**, 797-828.
7. L. G. H. Staaf, P. Lundgren and P. Enoksson, Present and Future Supercapacitor Carbon Electrode Materials for Improved Energy Storage Used in Intelligent Wireless Sensor Systems, *Nano Energy*, 2014, **9**, 128-141.
8. A. Izadi-Najafabadi, T. Yamada, D. N. Futaba, M. Yudasaka, H. Takagi, H. Hatori, S. Iijima and K. Hata, High-Power Supercapacitor Electrodes from Single-Walled Carbon Nanohorn/Nanotube Composite, *ACS Nano*, 2011, **5**, 811-819.
9. X. H. Cao, Y. M. Shi, W. H. Shi, G. Lu, X. Huang, Q. Y. Yan, Q. C. Zhang, H. Zhang, Preparation of Novel 3D Graphene Networks for Supercapacitor Applications, *Small*, 2011, **7**, 3163-3168.
10. L. L. Zhang, R. Zhou, X. S. Zhao, Graphene-based materials as supercapacitor electrodes, *J. Mater. Chem.*, 2010, **20**, 5983-5992.
11. C. Liu, Z. Yu, D. Neff, A. Zhamu and B. Z. Jang, Graphene-Based Supercapacitor with an Ultrahigh Energy Density, *Nano lett.*, 2010, **10**, 4863-4868.
12. T. F. Hsieh, C. C. Chuang, W. J. Chen, J. H. Huang, W. T. Chen and C. M. Shu, Hydrous Ruthenium Dioxide/Multi-Walled Carbon-Nanotube/Titanium Electrodes for Supercapacitors, *Carbon*, 2012, **50**, 1740-1747.
13. P. Li, Y. Yang, E. Shi, Q. Shen, Y. Shang, S. Wu, J. Wei, K. Wang, H. Zhu, Q. Yuan, A. Cao and D. Wu, Core-Double-Shell, Carbon Nanotube@Polypyrrole@MnO_2 Sponge as Freestanding, Compressible Supercapacitor Electrode, *ACS Appl. Mater. Interfaces*, 2014, **6**, 5228-5234.
14. I. Shakir, J. H. Choi, M. Shahid, S. A. Shahid, U. A. Rana, M. Sarfraz and D. J. Kang, Ultra-Thin and Uniform Coating of Vanadium Oxide on Multiwall Carbon Nanotubes through Solution Based

Approach for High-Performance Electrochemical Supercapacitors, *Electrochim. Acta*, 2013, **111**, 400-404.

15. J. Lang, X. Yan and Q. Xue, Facile Preparation and Electrochemical Characterization of Cobalt Oxide/Multi-Walled Carbon Nanotube Composites for Supercapacitors, *J. Power Sources*, 2011, **196**, 7841-7846.
16. P. X. Li, E. Z. Shi, Y. B. Yang, Y. Y. Shang, Q. Y. Peng, S. T. Wu, J. Q. Wei, K. L. Wang, H. W. Zhu, Q. Yuan, A. Y. Cao and D. H. Wu, Carbon Nanotube-Polypyrrole Core-Shell Sponge and Its Application as Highly Compressible Supercapacitor Electrode, *Nano Res.*, 2014, **7**, 209-218.
17. Z. Wang and C. J. Liu, Preparation and Application of Iron Oxide/Graphene Based Composites for Electrochemical Energy Storage and Energy Conversion Devices: Current Status and Perspective, *Nano Energy*, 2015, **11**, 277-293.
18. G. Binitha, M. S. Soumya, A. A. Madhavan, P. Praveen, A. Balakrishnan, K. R. V. Subramanian, M. V. Reddy, S. V. Nair, A. S. Nair and N. Sivakumar, Electrospun α-Fe_2O_3 Nanostructures for Supercapacitor Applications, *J. Mater. Chem. A*, 2013, **1**, 11698-11704.
19. H. C. Chen, C. C. Wang and S. Y. Lu, γ-Fe_2O_3/Graphene Nanocomposites as a Stable High Performance Anode Material for Neutral Aqueous Supercapacitors, *J. Mater. Chem. A*, 2014, **2**, 16955-16962.
20. Y. Zou, J. Kan and Y. Wang, Fe_2O_3-Graphene Rice-on-Sheet Nanocomposite for High and Fast Lithium Ion Storage, *J. Phys. Chem. C*, 2011, **115**, 20747-20753.
21. S. Yang, X. Song, P. Zhang and L. Gao, Heating-Rate-Induced Porous α-Fe_2O_3 with Controllable Pore Size and Crystallinity Grown on Graphene for Supercapacitors, *ACS Appl. Mater. Interfaces*, 2015, **7**, 75-79.
22. B. Koo, H. Xiong, M. D. Slater, V. B. Prakapenka, M. Balasubramanian, P. Podsiadlo, C. S. Johnson, T. Rajh and E. V. Shevchenko, Hollow Iron Oxide Nanoparticles for Application in Lithium Ion Batteries, *Nano lett.*, 2012, **12**, 2429-2435.
23. C. Guan, J. Liu, Y. Wang, L. Mao, Z. Fan, Z. Shen, H. Zhang and J. Wang, Iron Oxide-Decorated Carbon for Supercapacitor Anodes with Ultrahigh Energy Density and Outstanding Cycling Stability, *ACS Nano*, 2015, DOI: 10.1021/acsnano.5b00582.

24. Q. L. Shou, J. P. Cheng, L. Zhang, B. J. Nelson and X. B. Zhang, Synthesis and Characterization of a Nanocomposite of Goethite Nanorods and Reduced Graphene Oxide for Electrochemical Capacitors, *J. Solid State Chem.*, 2012, **185**, 191-197.

25. L. Xu, J. X. Xia, H. Xu, S. Yin, K. Wang, L. Y. Huang, L. G. Wang and H. M. Li, Reactable Ionic Liquid Assisted Solvothermal Synthesis of Graphite-like C_3N_4 Hybridized α-Fe_2O_3 Hollow Microspheres with Enhanced Supercapacitive Performance, *J. Power Sources*, 2014, **245**, 866-874.

26. Q. Qu, S. Yang and X. Feng, 2D Sandwich-Like Sheets of Iron Oxide Grown on Graphene as High Energy Anode Material for Supercapacitors, *Adv. Mater.*, 2011, **23**, 5574-5580.

27. L. F. Chen, Z. Y. Yu, X. Ma, Z. Y. Li and S. H. Yu, In Situ Hydrothermal Growth of Ferric Oxides on Carbon Cloth for Low-Cost and Scalable High-Energy-Density Supercapacitors, *Nano Energy*, 2014, **9**, 345-354.

28. P. Li, C. Kong, Y. Shang, E. Shi, Y. Yu, W. Qian, F. Wei, J. Wei, K. Wang, H. Zhu, A. Cao and D. Wu, Highly Deformation-Tolerant Carbon Nanotube Sponges as Supercapacitor Electrodes, *Nanoscale*, 2013, **5**, 8472-8479.

29. P. Chen, J. J. Yang, S. S. Li, Z. Wang, T. Y. Xiao, Y. H. Qian and S. H. Yu, Hydrothermal Synthesis of Macroscopic Nitrogen-Doped Graphene Hydrogels for Ultrafast Supercapacitor, *Nano Energy*, 2013, **2**, 249-256.

30. Y. Zhao, J. Liu, Y. Hu, H. Cheng, C. Hu, C. Jiang, L. Jiang, A. Cao and L. Qu, Highly Compression-Tolerant Supercapacitor Based on Polypyrrole-Mediated Graphene Foam Electrodes, *Adv. Mater.*, 2013, **25**, 591-595.

31. X. Gui, J. Wei, K. Wang, A. Cao, H. Zhu, Y. Jia, Q. Shu and D. Wu, Carbon Nanotube Sponges, *Adv. Mater.*, 2010, **22**, 617-621.

32. J. L. Li, K. N. Kudin, M. J. McAllister, R. K. Prud'homme, I. A. Aksay and R. Car, Oxygen-Driven Unzipping of Graphitic Materials, *Phys. Rev. Lett.*, 2006, **96**, 176101.

33. D. P. Yang, X. Wang, X. Guo, X. Zhi, K. Wang, C. Li, G. Huang, G. Shen, Y. Mei and D. Cui, UV/O_3 Generated Graphene Nanomesh: Formation Mechanism, Properties, and FET Studies, *J. Phys. Chem. C*, 2013, **118**, 725-731.

34. Z. Wang, D. Luan, S. Madhavi, Y. Hu and X. W. Lou, Assembling Carbon-coated α-Fe_2O_3 Hollow Nanohorns on the CNT Backbone for Superior Lithium Storage Capability, *Energy Environ. Sci.*, 2012, **5**, 5252-5256.

35. J. Zhong, Z. Yang, R. Mukherjee, A. Varghese Thomas, K. Zhu, P. Sun, J. Lian, H. Zhu and N. Koratkar, Carbon Nanotube Sponges as Conductive Networks for Supercapacitor Devices, *Nano Energy*, 2013, **2**, 1025-1030.

36. R. M. Cornell and U. Schwertmann, The Iron Oxides. Structure, Properties, Reactions, Occurrence and Uses, Wiley-VCH , 2003.

37. Y. Piao, J. Kim, H. B. Na, D. Kim, J. S. Baek, M. K. Ko, J. H. Lee, M. Shokouhimehr and T. Hyeon, Wrap-Bake-Peel Process for Nanostructural Transformation from β-FeOOH Nanorods to Biocompatible Iron Oxide Nanocapsules, *Nat. Mater.*, 2008, **7**, 242-247.

38. L. Li, Y. Chu, Y. Liu and L. Dong, Template-Free Synthesis and Photocatalytic Properties of Novel Fe_2O_3 Hollow Spheres, *J. Phys. Chem. C*, 2007, **111**, 2123-2127.

39. P. H. Yang, Y. Ding, Z. Y. Lin, Z. W. Chen, Y. Z. Li, P. F. Qiang, M. Ebrahimi, W. J. Mai, C. P. Wong and Z. L. Wang, Low-Cost High-Performance Solid-State Asymmetric Supercapacitors Based on MnO_2 Nanowires and Fe_2O_3 Nanotubes, *Nano lett.*, 2014, **14**, 731-736.

40. M. B. Sassin, A. N. Mansour, K. A. Pettigrew, D. R. Rolison and J. W. Long, Electroless Deposition of Conformal Nanoscale Iron Oxide on Carbon Nanoarchitectures for Electrochemical Charge Storage, *ACS Nano*, 2010, **4**, 4505-4514.

41. W. L. Yang, Z. Gao, J. Wang, B. Wang and L. H. Liu, Hydrothermal Synthesis of Reduced Graphene Sheets/Fe_2O_3 Nanorods Composites and Their Enhanced Electrochemical Performance for Supercapacitors, *Solid State Sci.*, 2013, **20**, 46-53.

42. W. M. Zhang, X. L. Wu, J. S. Hu, Y. G. Guo and L. J. Wan, Carbon Coated Fe_3O_4 Nanospindles as a Superior Anode Material for Lithium-Ion Batteries, *Adv. Funct. Mater.*, 2008, **18**, 3941-3946.

43. R. Wang, C. Xu, M. Du, J. Sun, L. Gao, P. Zhang, H. Yao and C. Lin, Solvothermal-Induced Self-Assembly of Fe_2O_3/GS Aerogels for High Li-Storage and Excellent Stability, *Small*, 2014, **10**, 2260-2269.

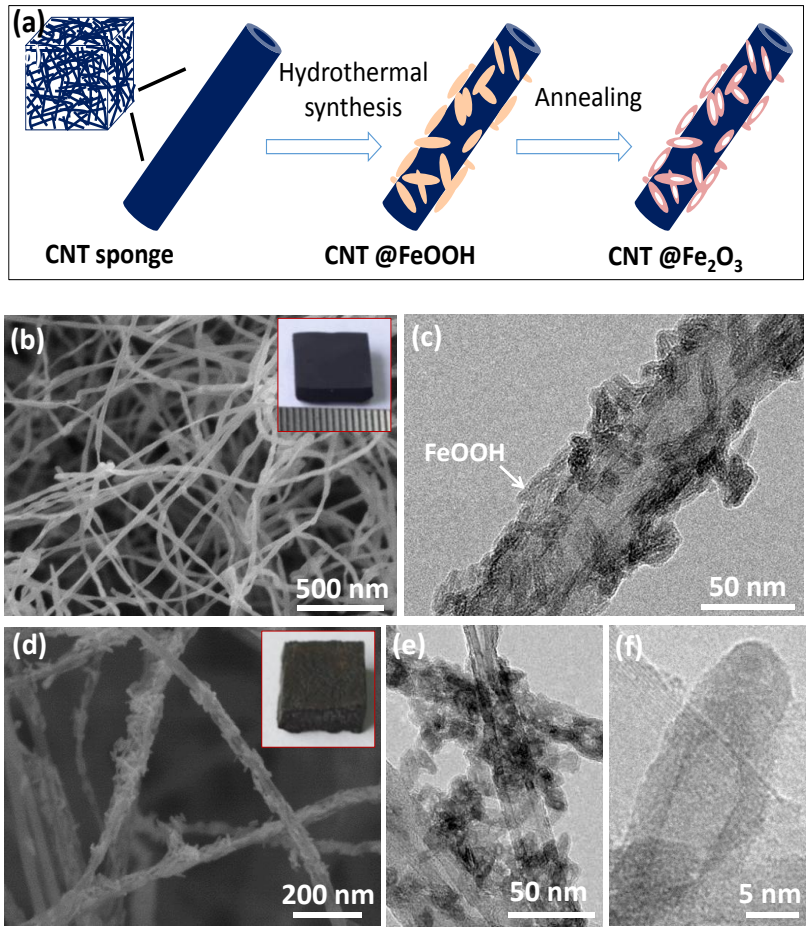

Fig. 1 Fabrication and morphology characterization of the CNT and CNT/Fe_2O_3 sponges. (a) illustration of the fabrication of the CNT@Fe_2O_3 sponge. (b) SEM image of the as-grown CNT sponge. Inset shows a sponge with the size of 11×10×3 mm. (c) TEM image of CNT@FeOOH showing uniform assembled FeOOH nanospindles on the surface of CNT. (d) SEM image of the CNT@Fe_2O_3 sponge. Inset shows a CNT@Fe_2O_3 sponge block. (e) and (f) TEM images of CNT@Fe_2O_3 showing hollow structure of rice-like Fe_2O_3 nanohorns.

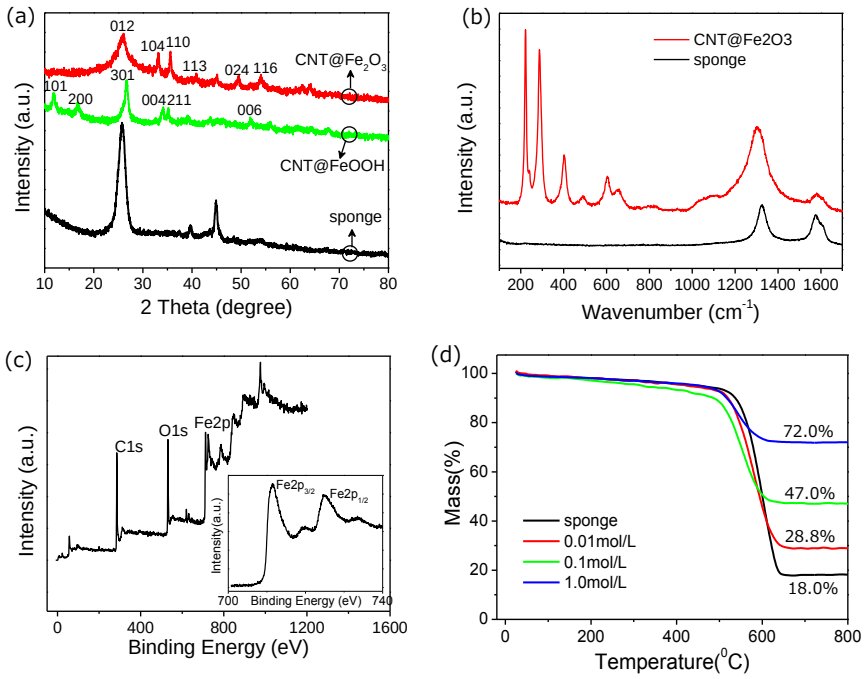

Fig. 2 Structural characterization of CNT and CNT@Fe_2O_3 sponges. (a) XRD patterns of CNT@Fe_2O_3, CNT@FeOOH and CNT sponges. (b) Raman spectra of CNT@Fe_2O_3 and CNT sponges. (c) XPS full spectrum of the CNT@Fe_2O_3 sponge showing three signals form Fe, O, and C elements. Inset is the high-resolution XPS spectra of Fe2p. (d) TGA analysis of the CNT sponge and three CNT@Fe_2O_3 sponges grown at different $FeCl_3$ precursor concentration.

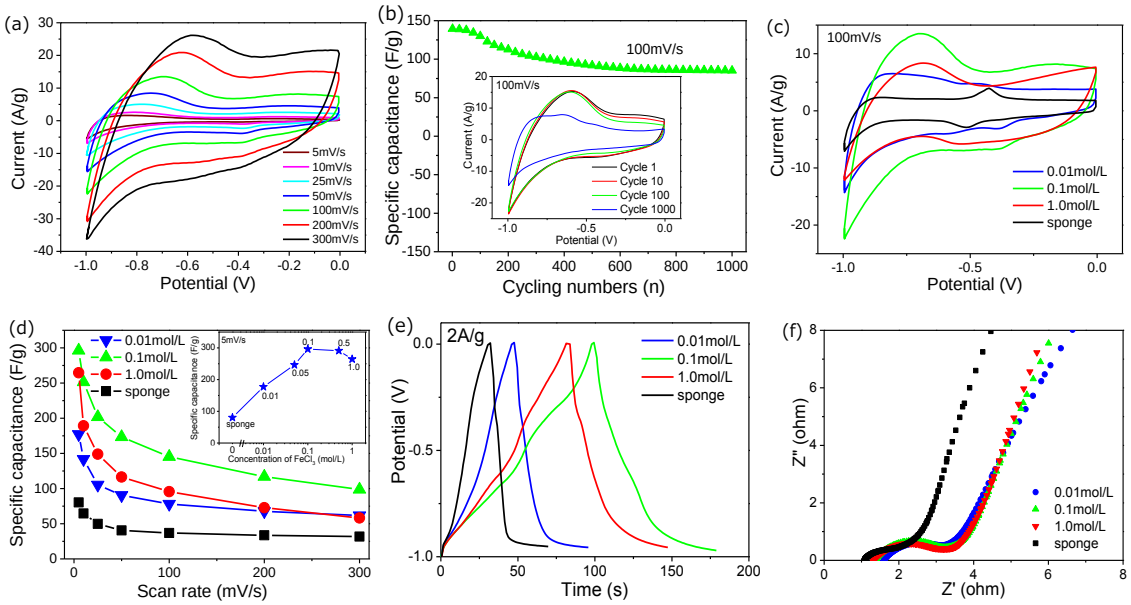

Fig. 3 Supercapacitor application of CNT@Fe_2O_3 sponges. (a) CV curves of CNT@Fe_2O_3 sponge at different scan rates from 5 to 300 mV/s. (b) The cycling performance of CNT@Fe_2O_3 sponge at a scan rate of 100 mV/s. Inset shows CV curves of the 1^{th}, 10^{th}, 100^{th}, and $1{,}000^{th}$ cycles. (c) CV curves of the CNT sponge and three CNT@Fe_2O_3 sponges grown at different $FeCl_3$ precursor concentration (0.01, 0.1 and 1.0 mol/L). (d) Calculated specific capacitances of the CNT sponge and three CNT@Fe_2O_3 sponges at different scan rates. Inset shows the specific capacitance of different samples at a scan rate of 5 mV/s. (e) Galvanostatic charge/discharge curves for the four samples. (f) Nyquist plot from electrochemical impedance test for different samples.

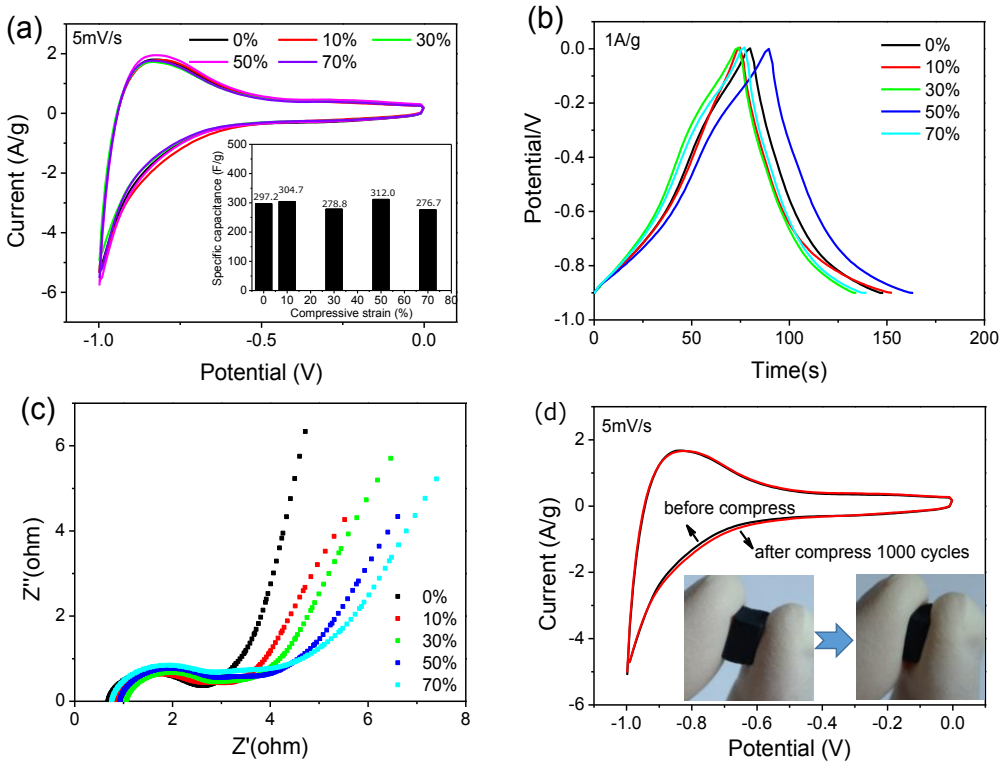

Fig. 4 Supercapacitor performance of the CNT@Fe_2O_3 under compression. (a) CV curves of CNT@Fe_2O_3 sponge under different compressed condition (ε=0%, 10%, 30%, 50% and 70%) at 5 mV/s. Inset shows the specific capacitance of the samples under different compressive strain at a scan rate of 5 mV/s. (b) Corresponding galvanostatic charge/discharge curves of CNT@Fe_2O_3 sponge under different compressive strain at a current of 1A/g. (c) Nyquist plot from electrochemical impedance test for different states. (d) CV cures of CNT@Fe_2O_3 sponge recorded before and after 1,000 compression cycles (ε= 50%) at 5 mV/s. Inset show pictures of the CNT@Fe_2O_3 sponge at original and pressed state.

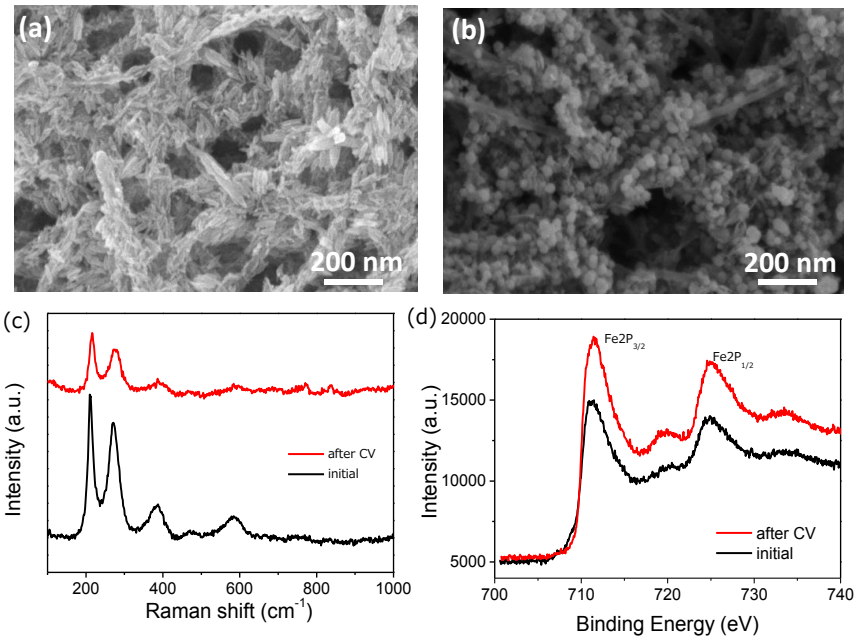

Fig. 5 Characterization of CNT@Fe_2O_3 sponges after electrochemical test. The electrochemical tests were conducted by CV at a scan rate of 100 mV/s. (a) SEM image of CNT@Fe_2O_3 in the initial state before the CV scan. (b) SEM image of CNT@Fe_2O_3 after 1000 cycles of the CV scan, showing spheroidizing and slight aggregation of the nanoparticles. (c) Raman spectra of CNT@Fe_2O_3 before and after the CV scan. (d) XPS spectra of CNT@Fe_2O_3 sponge before and after the CV scan.

Table of Contents of *TA-ART-05-2015-003635*

Three-dimensional α-Fe2O3/carbon nanotube sponges as flexible supercapacitor electrodes

Xiaoping Cheng[1], Xuchun Gui[1,*], Zhiqiang Lin[1], Yongjia Zheng[1], Ming Liu[1], Runze Zhan[1], Yuan Zhu[1] and Zikang Tang[1, 2]

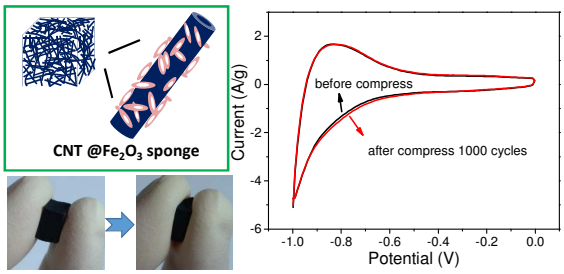

The porous, flexible and compressible CNT@Fe_2O_3 sponges show high specific capacitance (> 300 F/g).